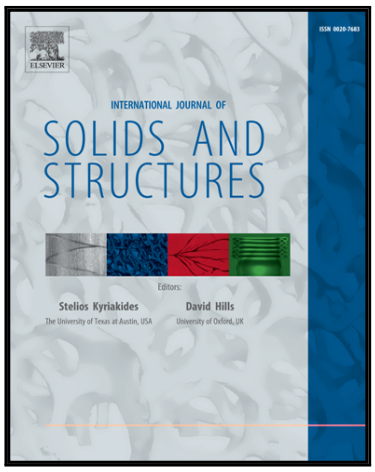

Large Deformation Analysis of Diffusion-Induced Buckling of Nanowires in Lithium-Ion Batteries

Kai Zhang , Yong Li , Bailin Zheng , Gangpeng Wu , Jingshen Wu , Fuqian Yang

PII: S0020-7683(16)30394-8
DOI: 10.1016/j.ijsolstr.2016.12.020
Reference: SAS 9406

To appear in: *International Journal of Solids and Structures*

Received date: 24 May 2016
Revised date: 12 December 2016
Accepted date: 22 December 2016

Please cite this article as: Kai Zhang , Yong Li , Bailin Zheng , Gangpeng Wu , Jingshen Wu , Fuqian Yang , Large Deformation Analysis of Diffusion-Induced Buckling of Nanowires in Lithium-Ion Batteries, *International Journal of Solids and Structures* (2016), doi: 10.1016/j.ijsolstr.2016.12.020

Large Deformation Analysis of Diffusion-Induced Buckling of Nanowires in Lithium-Ion Batteries

Kai Zhang[1], Yong Li[2, 3], Bailin Zheng[2], Gangpeng Wu[1], Jingshen Wu[1, *] and Fuqian Yang[3, *]

* Corresponding authors.

E-mail addresses: mejswu@ust.hk (J. Wu), fyang2@uky.edu (F. Yang).

1 Department of Mechanical and Aerospace Engineering, The Hong Kong University of Science and Technology, Clear Water Bay, Kowloon, Hong Kong

2 School of Aerospace Engineering and Applied Mechanics, Tongji University, No. 1239 Siping Road, Shanghai 200092, People's Republic of China

3 Department of Chemical and Materials Engineering, University of Kentucky, Lexington, Kentucky 40506, USA

Abstract: Buckling due to diffusion-induced compressive stress has been observed during the lithiation of various nanowires, and can affect the mechanical and electrochemical performance of nanowire-based electrodes. This study is focused on the diffusion-induced buckling of nanowires. Two diffusion paths are analyzed; one with radial diffusion only, and the other with axial diffusion. For the diffusion-induced buckling of nanowires with radial diffusion, the theory of large deformation is used in the description of the coupling between mass transport and deformation in large deformed solids. Using the linear theory, analytical solution of the critical length of a nanowire, below which there is no buckling, is obtained, which is dependent on the constraint of the ends of the nanowire and the volumetric strain of the nanowire at the fully lithiated state. The comparison between the linear analytical solution of the critical length and the numerical solution from the theory of large deformation shows that the linear analytical solution is valid for the influx less than 1 $mol \cdot m^{-2} \cdot s^{-1}$ and configurations considered in the work. Numerical analysis shows that the critical buckling time decreases with the increase of nanowire length and current density, and the nanowire

with two fixed ends has a larger critical buckling time than that for the same nanowire with a fixed end and a pinned end. The nanowire length plays a bigger role in determining the critical state of charge for the onset of the buckling than that of the diffusion flux. The state of charge (*SOC*) at the state of critical buckling decreases with the increase of the nanowire length and increases with the increase of current density. For the diffusion-induced buckling of nanowires with axial diffusion, numerical analysis is performed. The numerical result reveals similar trend, i.e., the critical buckling time decreases with the increase of nanowire length and current density. The comparison of the critical buckling times for the conditions with axial diffusion, radial diffusion and diffusion from all sides, respectively, reveals that the contribution from axial diffusion is negligible even for small aspect ratio, and it does not change significantly with the increase of the aspect ratio.

Keywords: nanowire; diffusion-induced stress; buckling; large deformation.

1. Introduction

The continuous development in science and technology has increased the demand of energy storage devices for our daily life. Lithium-ion batteries (LIBs) have recently attracted great attention because of their high energy capacity and long cycle life. The electrochemical performance of LIBs is crucially related to the materials behavior of electrodes. It has been demonstrated that nanowire-based electrodes exhibit high electrochemical performance since they can accommodate large strain without significant pulverization, provide good electrical contact and electronic conduction, and have short distance for the lithium diffusion (Chan et al., 2008).

It is known that the lithiation or delithiation of an electrode will lead to volumetric change. The inhomogeneous change of volume will introduce local stress in the electrode, which is referred to as diffusion-induced stress (DIS). In general, the diffusion-induced stress can be either tensile or compressive. Under the action of compressive stress, a slender structure, such as the nanowires or nanotubes used in LIBS, will experience buckling when the compressive stress is larger than or equal to the critical stress. Such behavior has been observed during the lithiation of Al nanowires (Liu et al., 2011), Si nanowires (Cui, 2011; Liu et al., 2013), and SnO_2 nanowires (Huang et al., 2010; Zhong et al., 2011). The diffusion-induced buckling can degrade the mechanical integrity of the slender structure (nanowires or nanotubes), which plays an important role in controlling the electrochemical performance of the electrodes in LIBs. It is of practical importance to study the diffusion-induced stresses in nanowires and their effect on the buckling behavior of the nanowires.

Prussin (Prussin, 1961) in investigating the effect of dopant on the stress evolution in silicon was likely the first one to use a thermal-analogy method and obtain the stress induced by the impurity in a Si plate,. Recently, there is a great interest of using the concept of DIS to analyze the stress evolution in the electrodes of LIBs due to lithiation and delithiation. Zhang et al. (Zhang et al., 2008; Zhang et al., 2007) systematically studied the intercalation-induced stresses in spherical and ellipsoidal particles, in which they considered the contribution of hydrostatic stress to chemical potential similar to the formula used by Li (Li, 1978) and Yang (Yang, 2005). Cheng et al. (Cheng and Verbrugge, 2008) examined the effect of surface

tension and surface modulus on diffusion-induced stresses in spherical nanoparticles. They found that surface mechanics plays a great role in determining the magnitude and distribution of stresses in a nanoscale particle. Cui et al. (Cui et al., 2012) investigated the insertion/extraction of lithium ions into/out a silicon particle by using a stress-dependent chemical potential and the theory of large deformation. Zhao et al. (Zhao et al., 2011) developed a theory of finite plastic deformation of an electrode caused by electrochemical charging and discharging and analyzed the stresses in the electrode within nonequilibrium thermodynamics. Yang (Yang, 2010) considered the effect of local solid reaction on diffusion-induced stress and derived a general relationship among the concentration of solute atoms, local reaction product, and mechanical stress. Bhandakkar and Gao (Bhandakkar and Gao, 2010) developed a cohesive model of crack nucleation in an initially crack-free strip electrode under galvanostatic charging and discharging. Using a theory of concurrent large swelling and finite-strain plasticity, Brassart et al. (Brassart et al., 2013) simulated the field evolution in an electrode subject to cyclic lithiation and delithiation.

There are only a few studies addressing the effect of diffusion-induced stresses on the buckling of the structures in the electrode of LIBs. Bhandakkar and Johnson (Bhandakkar and Johnson, 2012) analyzed the diffusion-induced stresses in honeycomb-like electrodes, which undergoes elastic-plastic deformation during cycling and found that the honeycomb-like geometry allows for the presence of buckling deformation. Zhang and Zhao (Zhang and Zhao, 2012) depicted the stresses provenance and evolution of hollow nanosphere and nanotube induced by the diffusion of lithium ions, in which they considered self-buckling induced by surface stresses and analyzed critical buckling sizes. Chakraborty et al. (Chakraborty et al., 2015) presented a general framework to study the mechanical behavior of a cylindrical silicon anode particle with two boundaries; one is traction-free for all surfaces and the other is axially-restrained for the cylindrical particle. They observed the occurrence of buckling due to the compressive axial stress for the axially-restrained condition, and obtained a critical length below which the cylinder will never buckle. However, none of these studies has studied the factors controlling the onset of buckling and the effect of diffusion paths.

This work is focused on the diffusion-induced buckling of a nanowire. First, the theory of large deformation is used to investigate the diffusion-induced buckling of the nanowire with

radial diffusion. The interaction between stress and diffusion is considered in the analysis. The effects of the aspect ratio of the nanowire, electric current density, and boundary conditions on the critical time are discussed for the onset of the buckling. Secondly, a relationship between the critical length of a nanowire, below which the nanowire will never buckle, and material properties is established, following the study given by Chakraborty et al. (Chakraborty et al., 2015) and using the theory of linear elasticity. Finally, finite element method (FEM) is used to analyze the diffusion-induced buckling of a nanowire with axial diffusion. The effects of the nanowire length and current density are discussed. It is worth pointing out that the PDE (partial differential equation) module in COMSOL multiphysics is used first to solve the diffusion and deformation problems numerally, and the commercial FEM program of ABAQUS is used to solve the post-buckling problem and the problem associated with axial diffusion.

2. Diffusion-induced buckling of a nanowire with radial diffusion

2.1 Mechanical equations

The insertion of solute atoms into a host material will cause the change of the distance between adjacent atoms of the host material near the solute atoms, resulting in local deformation/strain. For large deformation, there are two approaches to describe the deformation, i.e., the Lagrangian description and the Eulerian description. The Lagrangian description is based on the initial state, and uses **X** as the coordinates. The Eulerian description is based on the current state, and uses **x** as the corresponding coordinates. There exists one-to-one mapping between these two descriptions as

$$\mathbf{x} = \chi(\mathbf{X}, t), \tag{1}$$

$$\mathbf{X} = \chi^{-1}(\mathbf{x}, t), \tag{2}$$

where χ represents a uniquely invertible vector field associated with the motion of the material.

In the Lagrangian description, the displacement vector of **U** is calculated as

$$\mathbf{U}(\mathbf{X}, t) = \mathbf{x}(\mathbf{X}, t) - \mathbf{X}. \tag{3}$$

and the deformation gradient tensor of **F** in terms of the displacement vector is calculated as

$$\mathbf{F} = \mathrm{Grad}\mathbf{x} = \mathbf{I} + \mathrm{Grad}\mathbf{U}\left(\mathbf{X}, t\right), \tag{4}$$

where Grad is the gradient operator in the Lagrangian description, and **I** is the unit tensor of second order.

Consider an electrode made of a nanowire with an initial radius of R_0 in a cylindrical coordinate system (r, θ, z) in the Eulerian description, as shown in Fig. 1. The corresponding coordinate system in the Lagrangian description is (R, Θ, Z). Using the axisymmetric characteristic of the problem, the resultant deformation gradient tensor, **F**, in the Lagrangian description is written as

$$\mathbf{F} = \begin{bmatrix} F_R & 0 & 0 \\ 0 & F_\Theta & 0 \\ 0 & 0 & F_Z \end{bmatrix} = \begin{bmatrix} 1+\partial u/\partial R & 0 & 0 \\ 0 & 1+u/R & 0 \\ 0 & 0 & 1+\partial w/\partial Z \end{bmatrix}, \tag{5}$$

where u is the radial displacement, and w is the axial displacement.

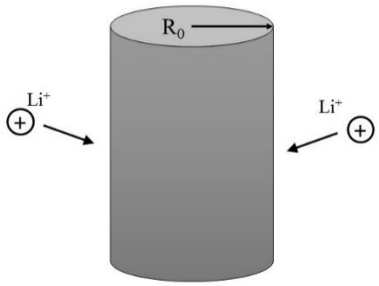

Figure 1. Schematic of a nanowire electrode with radial diffusion

The total deformation gradient tensor, **F**, consists of the elastic deformation tensor, $\mathbf{F}^e$, and the inelastic deformation tensor, $\mathbf{F}^i$, as

$$\mathbf{F} = \mathbf{F}^e\mathbf{F}^i. \tag{6}$$

Assuming that the inelastic deformation, which is introduced by the insertion or de-insertion of solute atoms, is isotropic, the inelastic deformation gradient tensor can be written as (Cui et al., 2012)

$$\mathbf{F}^i = \left(1+\Omega_1 C\right)^{1/3}\mathbf{I}, \tag{7}$$

with C being the concentration of the solute atoms in the Lagrangian description and Ω_1 being the volumetric strain per unit mole fraction of the solute atoms.

The elastic deformation gradient tensor, $\mathbf{F}^e$, in the cylindrical coordinate in the Lagrangian description is

$$\mathbf{F}^e = \left(1+\Omega_1 C\right)^{-1/3}\begin{bmatrix} 1+\partial u/\partial R & 0 & 0 \\ 0 & 1+u/R & 0 \\ 0 & 0 & 1+\partial w/\partial Z \end{bmatrix}. \quad (8)$$

Using the Green-Lagrange strain tensor, the components of the elastic strain tensor, $\mathbf{E}^e$, is calculated as

$$E_R^e = \frac{1}{2}\left[\frac{\left(1+\partial u/\partial R\right)^2}{\left(1+\Omega_1 C\right)^{2/3}} - 1\right], \quad (9)$$

$$E_\Theta^e = \frac{1}{2}\left[\frac{\left(1+u/R\right)^2}{\left(1+\Omega_1 C\right)^{2/3}} - 1\right], \quad (10)$$

$$E_Z^e = \frac{1}{2}\left[\frac{\left(1+\partial w/\partial Z\right)^2}{\left(1+\Omega_1 C\right)^{2/3}} - 1\right]. \quad (11)$$

Following the approach used by Cui et al. (Cui et al., 2013), the constitutive relation for the deformation is determined from the strain energy density as

$$\mathbf{P} = \frac{\partial W}{\partial \mathbf{F}} = \frac{\partial W}{\partial \mathbf{E}^e}\frac{\partial \mathbf{E}^e}{\partial \mathbf{F}^e}\frac{\partial \mathbf{F}^e}{\partial \mathbf{F}}, \quad (12)$$

where $\mathbf{P}$ is the first Piola-Kirchhoff stress and W is the elastic strain energy density in the Lagrangian description. There are reports on the description of the constitutive behavior of silicon in the battery environment (Areias et al., 2016; Barai and Mukherjee, 2016; Damle et al., 2016; Gao and Hong, 2016; Wang and Xiao, 2016), in which the elastic strain energy density is expressed as a quadratic function of the Green-Lagrange strain tensor, i.e.

$$W = \det\left(\mathbf{F}^i\right)\frac{E_h}{2\left(1+\nu\right)}\left[\frac{\nu}{\left(1-2\nu\right)}\left[tr\left(\mathbf{E}^e\right)\right]^2 + tr\left(\mathbf{E}^e\mathbf{E}^e\right)\right]. \quad (13)$$

where E_h and ν are Young's modulus and Poisson's ratio of the nanowire, respectively, $\det(\mathbf{F}^i)$ is the determinant of the inelastic deformation gradient tensor, and *tr* is the trace of the tensor. Substituting Eq. (13) into Eq. (12) yields

$$\mathbf{P} = \det\left(\mathbf{F}^i\right)\frac{E_h}{2\left(1+\nu\right)}\left[\frac{\nu}{\left(1-2\nu\right)}tr\left(\mathbf{E}^e\right) + 2\mathbf{E}^e\right]\mathbf{F}^e\left(\mathbf{F}^i\right)^{-1}. \quad (14)$$

Substituting Eqs. (7)-(11) into Eq. (14), one obtains the components of the first Piola-Kirchhoff stress tensor as

$$P_R = \left(1+\Omega_1 C\right)^{1/3} \frac{\nu}{\left(1+\nu\right)\left(1-2\nu\right)} E_h \left(\frac{1-\nu}{\nu} E_R^e + E_\Theta^e + E_Z^e \right)\left(1+\frac{\partial u}{\partial R}\right), \tag{15}$$

$$P_\Theta = \left(1+\Omega_1 C\right)^{1/3} \frac{\nu}{\left(1+\nu\right)\left(1-2\nu\right)} E_h \left(E_R^e + \frac{1-\nu}{\nu} E_\Theta^e + E_Z^e \right)\left(1+\frac{u}{R}\right), \tag{16}$$

$$P_Z = \left(1+\Omega_1 C\right)^{1/3} \frac{\nu}{\left(1+\nu\right)\left(1-2\nu\right)} E_h \left(E_R^e + E_\Theta^e + \frac{1-\nu}{\nu} E_Z^e \right)\left(1+\frac{\partial w}{\partial Z}\right). \tag{17}$$

The equilibrium equation at quasi-static state in the absence of body force is

$$\frac{\partial P_R}{\partial R} + \frac{P_R - P_\Theta}{R} = 0. \tag{18}$$

The axisymmetric characteristic of the problem gives the following boundary condition

$$u\left(0,t\right) = 0. \tag{19}$$

The traction-free condition on the outer surface of the nanowire is

$$P_R\left(R_0,t\right) = 0. \tag{20}$$

For a nanowire with the length much larger than radius, the deformation state of the nanowire can be approximated as plane strain, and the axial Green-Lagrange strain is equal to zero, i.e.

$$\frac{\partial w}{\partial Z} = 0. \tag{21}$$

The resultant axial force, F_z, acting on the nanowire is calculated as

$$F_Z = \int_0^{2\pi} \int_0^{R_0} P_Z R dR d\Theta. \tag{22}$$

It is known that a slender structure (nanowire) can experience buckling under the action of an axial, compressive force. During the lithiation process, the nanowire begins to expand both in the radial direction and the axial direction. If both ends of the nanowire are immobile along the axial direction, the lithiation will introduce an axial, compressive force, resulting in the onset of the buckling of the nanowire when the axial, compressive force is larger than the critical load. From the theory of linear elasticity (Gere and Goodno, 2009), the critical load, F_{cr}, for the onset of the buckling of the nanowire, known as Euler's critical load, can be calculated as

$$F_{cr} = -\frac{\pi^2 E_h I}{\left(\chi L\right)^2}, \tag{23}$$

where I ($=\pi R_0^4/4$) is the inertia moment of the nanowire, and L is the length of the nanowire.

The constant of χ is dependent on the boundary conditions at both ends of the nanowire. There are χ = 0.7 for a nanowire with a fixed end and a pinned end, and χ = 0.5 for a nanowire with two fixed ends. Note that De Pascalis et al. (De Pascalis et al., 2011) had shown that the Euler critical buckling load derived from small deformation is applicable to the buckling of thin enough cylinders in large deformation by asymptotic analysis. The detailed validation is given in Appendix C.

From Eq. (23), the condition for the onset of the diffusion-induced buckling of a nanowire is

$$F_Z = F_{cr}, \tag{24}$$

which gives

$$\int_0^{2\pi}\int_0^{R_0} P_Z R dR d\Theta = -\frac{\pi^2 E_h I}{(\chi L)^2}. \tag{25}$$

2.2 Diffusion equations

Similar to the deformation analysis of materials, there are two frameworks, i.e. Lagrangian description and Eulerian description, used to describe the flow (diffusion) field of materials. In the Eulerian framework, the flow field is described as functions of time and of fixed space coordinates and calculated at fixed points in space as time varies. In the Lagrangian framework, the positions of moving particles (atoms) are described by functions of time and of their initial positions or any set of material functions of moving particles (atoms) (Grushka and Grinberg, 2014). Fyrillas and Nomura (Fyrillas and Nomura, 2007) had given the convection-diffusion partial differential equation in both the Lagrangian and Eulerian frameworks, which can be used to describe the diffusion problem in both frameworks if the convection term is assumed as zero.

Recently, Li et al. (Li et al., 2016) analyzed the mass transport accounting for the stress-induced diffusion in both the Lagrangian description and the Eulerian description. For completeness, we briefly describe the diffusion equations in both systems. Define **J** as the resultant flux of solute atoms, which is a function of the coordinates, **X**, and time, *t*, in the Lagrangian description. The conservation of solute atoms in the absence of any solid reaction gives

$$\frac{\partial C}{\partial t} + \mathrm{Div}\mathbf{J} = 0. \tag{26}$$

The concentration, c, and resultant flux, $\mathbf{j}$, in the Eulerian description can be calculated from their Lagrangian counterparts as $C=\det(\mathbf{F})c$ and $\mathbf{J}=\det(\mathbf{F})\mathbf{j}\mathbf{F}^{-T}$, respectively.

For a cylindrical electrode, Eq. (26) is reduced to

$$\frac{\partial C(R,t)}{\partial t} + \frac{\partial\left(RJ(R,t)\right)}{R\partial R} = 0. \tag{27}$$

It needs to point out that the kinematics of solute atoms should be analyzed in the Eulerian description, which is based on the current state. From the theory of kinetics, the diffusion flux is

$$\mathbf{j} = -Mc\,\mathrm{grad}\mu, \tag{28}$$

where μ is chemical potential, grad is the gradient operator in the Eulerian description, and M is the mobility of the solute atoms.

The chemical potential for a dilute solution is written as (Larché, 1996; Larché and Cahn, 1985)

$$\mu = \mu_0 + R_g T \ln c - \sigma_m \Omega_1 + w\Omega_2, \tag{29}$$

where μ_0 is the chemical potential at a reference state, R_g is the gas constant, T is absolute temperature, σ_m is the Cauchy hydrostatic stress in the Eulerian description, Ω_2 is the partial molar volume of the solute atoms, and w is the strain energy density in the Eulerian description. The Cauchy hydrostatic stress is

$$\begin{aligned}\sigma_m &= \frac{1}{3}tr(\boldsymbol{\sigma}) = \frac{1}{3}tr\left(\det{}^{-1}(\mathbf{F})\mathbf{P}\mathbf{F}^T\right)\\ &= \frac{1}{3}tr\left\{\frac{\det(\mathbf{F}^i)}{\det(\mathbf{F})}\frac{E_h}{2(1+\nu)}\left[\frac{\nu}{(1-2\nu)}tr(\mathbf{E}^e)+2\mathbf{E}^e\right]\mathbf{F}^e(\mathbf{F}^i)^{-1}\mathbf{F}^T\right\},\end{aligned} \tag{30}$$

and the strain energy density in the Eulerian description is

$$w = \frac{W}{\det(\mathbf{F}^i)} = \frac{E_h}{2(1+\nu)}\left[\frac{\nu}{(1-2\nu)}\left[tr(\mathbf{E}^e)\right]^2 + tr(\mathbf{E}^e\mathbf{E}^e)\right]. \tag{31}$$

Substituting Eqs. (29)-(31) into Eq. (28) yields

$$\mathbf{j}=-Mc\,\mathrm{grad}\left\{\mu_0+R_gT\ln c+\frac{\Omega_2 E_h}{2(1+\nu)}\left[\frac{\nu}{(1-2\nu)}\left[tr\left(\mathbf{E}^e\right)\right]^2+tr\left(\mathbf{E}^e\mathbf{E}^e\right)\right]-\frac{\Omega_1}{3}tr\left\{\frac{\det\left(\mathbf{F}^i\right)}{\det\left(\mathbf{F}\right)}\frac{E_h}{2(1+\nu)}\left[\frac{\nu}{(1-2\nu)}tr\left(\mathbf{E}^e\right)+2\mathbf{E}^e\right]\mathbf{F}^e\left(\mathbf{F}^i\right)^{-1}\mathbf{F}^T\right\}\right\}. \tag{32}$$

Using the equations of $C=\det(\mathbf{F})c$ and $\mathbf{J}=\det(\mathbf{F})\mathbf{j}\mathbf{F}^{-T}$, the diffusion flux in the Lagrangian description is expressed as

$$\mathbf{J}=-\left(\mathbf{F}^{-T}\right)^2 MC\mathrm{Grad}\left\{\mu_0+R_gT\ln\frac{C}{\det\left(\mathbf{F}\right)}+\frac{\Omega_2 E_h}{2(1+\nu)}\left[\frac{\nu}{(1-2\nu)}\left[tr\left(\mathbf{E}^e\right)\right]^2+tr\left(\mathbf{E}^e\mathbf{E}^e\right)\right]-\frac{\Omega_1}{3}tr\left\{\frac{\det\left(\mathbf{F}^i\right)}{\det\left(\mathbf{F}\right)}\frac{E_h}{2(1+\nu)}\left[\frac{\nu}{(1-2\nu)}tr\left(\mathbf{E}^e\right)+2\mathbf{E}^e\right]\mathbf{F}^e\left(\mathbf{F}^i\right)^{-1}\mathbf{F}^T\right\}\right\}. \tag{33}$$

Substituting Eqs. (5)-(11) into Eq. (33), one obtains the radial component of the diffusion flux as

$$J\left(R,t\right)=-\left(\frac{1}{1+\frac{\partial u}{\partial R}}\right)^2\frac{D}{R_gT}C\frac{\partial}{\partial R}\left\{\mu_0+R_gT\ln\frac{C}{\left(1+\frac{\partial u}{\partial R}\right)\left(1+\frac{u}{R}\right)\left(1+\frac{\partial w}{\partial Z}\right)}-\frac{1}{3}\Omega_1\left[\frac{P_R}{\left(1+\frac{u}{R}\right)\left(1+\frac{\partial w}{\partial Z}\right)}+\frac{P_\Theta}{\left(1+\frac{\partial u}{\partial R}\right)\left(1+\frac{\partial w}{\partial Z}\right)}+\frac{P_Z}{\left(1+\frac{\partial u}{\partial R}\right)\left(1+\frac{u}{R}\right)}\right]+\frac{\Omega_2 E_h}{2(1+\nu)}\left[\frac{\nu}{1-2\nu}\left(E_R^e+E_\Theta^e+E_Z^e\right)^2+\left(E_R^e\right)^2+\left(E_\Theta^e\right)^2+\left(E_Z^e\right)^2\right]\right\}, \tag{34}$$

where $D(=R_gTM)$ is the diffusion coefficient.

The diffusion equation in the Lagrangian description can be obtained by substituting Eq. (34) into Eq. (27).

For galvanostatic charging, the boundary condition in the Eulerian description is

$$\mathbf{j}\left(\mathbf{x},t\right)\mathbf{n}\big|_{r=r_0(t)}=\mathbf{j}_0\mathbf{n},\quad t>0, \tag{35}$$

and the corresponding boundary condition in the Lagrangian description is

$$\mathbf{J}\left(\mathbf{X},t\right)\mathbf{N}\big|_{R=R_0}=\det\left(\mathbf{F}\right)\mathbf{j}_0\mathbf{F}^{-T}\mathbf{N},\quad t>0, \tag{36}$$

where the magnitude of $\mathbf{j}_0$ is proportional to the current density, $\mathbf{n}$ is the unit normal vector in

the Eulerian description, and **N** is the unit normal vector in the Lagrangian description.

The initial condition for the nanowire without solute atoms incipiently in the Eulerian description is

$$c(\mathbf{x},0)=0, \quad 0<\mathbf{x}<\mathbf{x}_0(t), \tag{37}$$

and the corresponding initial condition in the Lagrangian description is

$$C(\mathbf{X},0)=0, \quad 0<\mathbf{X}<\mathbf{X}_0. \tag{38}$$

For a cylindrical electrode, the boundary condition becomes

$$J(R_0,t)=\left(1+\frac{u}{R}\right)\left(1+\frac{\partial w}{\partial Z}\right)j_0. \tag{39}$$

and the initial condition becomes

$$C(R,0)=0, \quad 0\le R\le R_0. \tag{40}$$

Solving the coupling equations of deformation, diffusion, and Eq. (25), one can determine the critical diffusion time and the distribution of the critical lithium concentration for the onset of the buckling of a nanowire during lithiation. Note that the end effect is neglected in the following analysis.

2.3 Numerical analyses

Numerical analyses were used to solve the above equations and calculate the critical diffusion time and the distribution of the critical lithium concentration for the lithiation-induced buckling of a nanowire. The numerical calculation of the above equations was performed using the PDE module in the COMSOL multiphysics software. The nanowire was assumed to be a silicon nanowire. The self-limiting behavior (Drozdov, 2014; Liu et al., 2013) was not considered in the analysis. Table I lists the material properties and parameters used in the numerical analyses.

The PDE module in the COMSOL was used to solve the evolution of stresses and the Li-concentration, from which the critical buckling time was calculated using Euler's critical load. A time-dependent step was conducted with the time step of $0.001Dt/R_0^2$, and the linear 2-node element was used with the element size of $R_0/400$. Both of them were small enough to ensure the convergence of the numerical results and the calculation accuracy. Generally, the

post-buckling analysis can reveal the critical time for the onset of the buckling induced by the diffusion of lithium. Using the commercial finite element software of ABAQUS, the post-buckling analysis was performed. The FEM results were compared to the results from the Euler's critical load to verify the viability of the linear theory. The comparison was given in Appendix A.

Note that the numerical calculation of the resultant axial force was performed by the software itself.

Table I. Material properties of silicon nanowire and the parameters used in the calculation

Parameter	Symbol	Value
Young's modulus	E_h	90 *GPa* (Pal et al., 2014)
Poisson's ratio	ν	0.28 (Pal et al., 2014)
Volumetric strain per unit mole fraction of lithium in silicon	Ω_1	$8.18\times10^{-6}\ m^3\cdot mol^{-1}$ (Zhao et al., 2011)
Partial molar volume	Ω_2	$8.18\times10^{-6}\ m^3\cdot mol^{-1}$ (Zhao et al., 2011)
Gas constant	R_g	$8.31\ J\cdot mol^{-1}\cdot K^{-1}$
Diffusion coefficient	D	$10^{-16}\ m^2\cdot s^{-1}$ (Pal et al., 2014)
Temperature	T	300 *K*
Cylindrical radius	R_0	$5\times10^{-8}\ m$ (Chan et al., 2008)

Figure 2 shows the variation of the critical buckling time with the parameter j_0 for the onset of the buckling of nanowires with a fixed end and a pinned end for different ratios of length to radius. The dimensionless time τ ($=Dt/R_0^2$) was used. It is evident that the critical buckling time decreases nonlinearly with the increasing values of j_0 for the same nanowire, as expected, since a larger value of j_0 will lead to a larger amount of solute atoms into the nanowire according to Eq. (34) and (39), resulting in a larger axial, compressive force for the onset of the buckling. Such nonlinear behavior reveals the interaction between diffusion and stress.

Figure 3 depicts the variation of the critical buckling time with the ratio of length to radius for different values of j_0 for the onset of the buckling of nanowires with a fixed end and a pinned end. For the same value of j_0, the critical buckling time decreases with the

increase of the ratio of length to radius, suggesting that a nanowire with a smaller ratio of length to radius can accommodate a larger amount of solute atoms before the onset of the buckling in accord with a larger critical force for the onset of the buckling. Such a result is in agreement with Eq. (23) that a smaller critical buckling force is needed to initiate the buckling of a longer nanowire of the same radius.

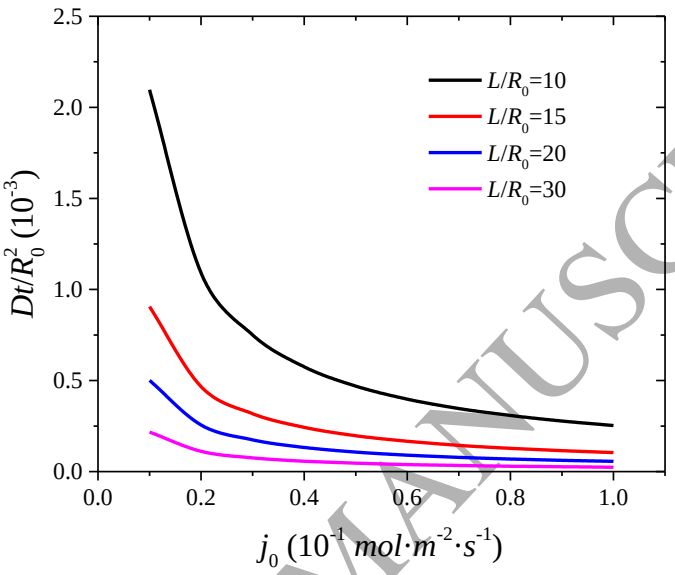

Figure 2. Variation of the critical buckling time with the parameter of j_0 for the onset of the buckling of nanowires with a fixed end and a pinned end for different ratios of length to radius

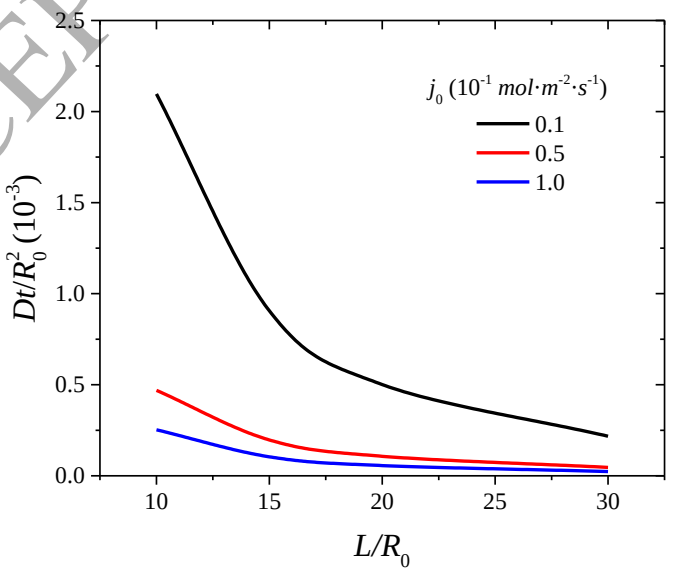

Figure 3. Variation of the critical buckling time with the ratio of length to radius for different values of j_0 for the onset of the buckling of nanowires with a fixed end and a pinned end

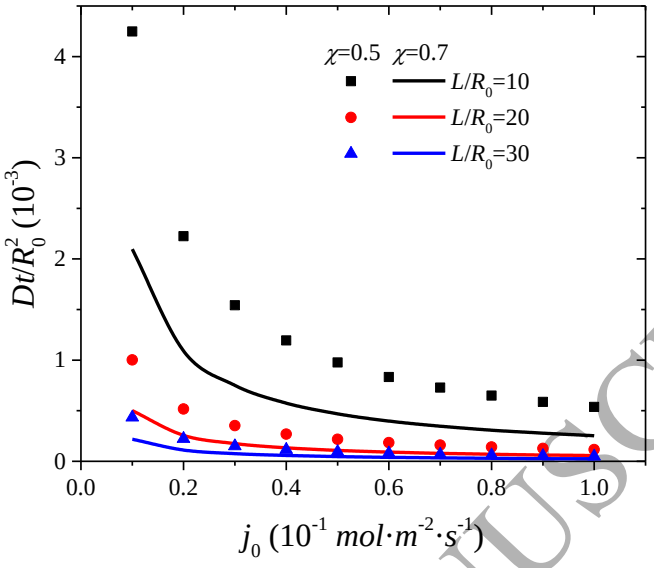

Figure 4. Variation of the critical buckling time with the parameter of j_0 for the onset of the buckling for nanowires with different ratios of length to radius under two different constraint conditions (Solid lines represent the nanowires with a fixed end and a pinned end; symbols represent the nanowires with two fixed ends.)

As discussed above, the critical load for the onset of the buckling is dependent on the constraints on the both ends of a slender structure. Figure 4 shows the comparison of the critical buckling times for nanowires subjected to different constraints: one with a fixed end and a pinned end (solid lines), and the other with two fixed end (symbols). For a nanowire with the same ratio of length to radius, a larger critical buckling time is needed for the onset of the buckling of the nanowire with two fixed ends than that with a fixed end and a pinned end, as expected, since a larger Euler's critical load corresponds to a smaller value of χ according to Eq. (23). For nanowires with larger ratios of length to radius, the difference between the two critical buckling times becomes smaller due to the less effect of the constraints on the deformation of the nanowires.

In general, it is desirable for electrodes to accommodate more lithium. It is of practical importance to determine the factors determining the storage capacity of lithium before the onset of buckling in addition to the examination of the factors determining the critical

buckling time of nanowires. The state of charging (*SOC*), which represents the percentage of full capacity, is defined as

$$SOC = \int_0^{R_0} C(R,t)\,RdR \left[\int_0^{R_0} C_{\max} RdR\right]^{-1}, \tag{41}$$

where $C_{\max}$ is the maximum stoichiometric concentration of lithium in a material. For homogeneous cylinders, $C_{\max}$ is position-independent, and *SOC* can be calculated as

$$SOC = \frac{2\int_0^{R_0} C(R,t)\,RdR}{C_{\max} R_0^2}. \tag{42}$$

Figure 5 shows the variation of *SOC* with the ratio of length to radius and the parameter of j_0 at the onset of buckling with the condition of a fixed end and a pinned end. For a nanowire subjected to constant diffusion influx, the *SOC* at the onset of buckling decreases with increasing the ratio of length to radius, indicating that reducing the aspect ratio of nanowires can lead to the increase of the storage capacity of lithium before the onset of buckling. For a nanowire with the same ratio of length to radius, the *SOC* at the onset of buckling increases with increasing the diffusion influx. Such behavior is because a higher influx leads to a sharp concentration gradient near the surface, and more Li diffuse into the nanowire in a short time, resulting in a high *SOC* value at the onset of buckling. For nanowires with large ratios of length to radius, the SOC at the onset of buckling becomes less dependent on the diffusion flux.

(a)

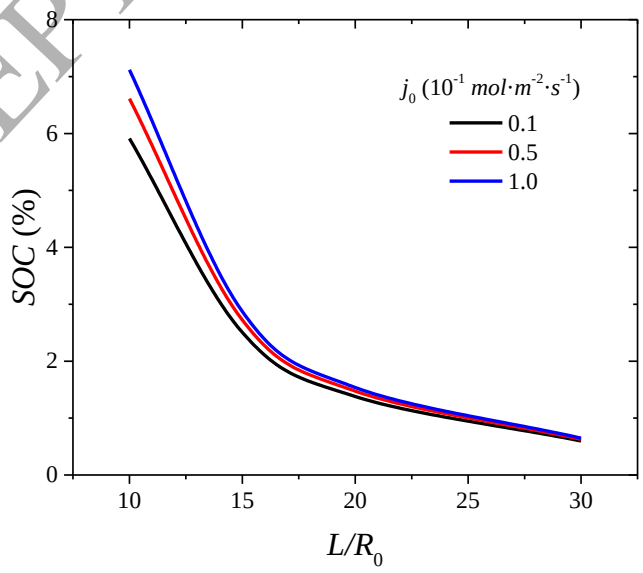

(b)

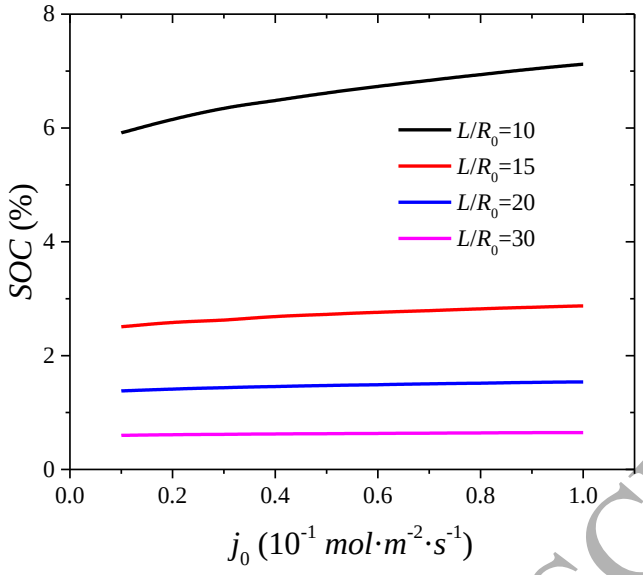

Figure 5. Variation of *SOC* with (a) the ratio of length to radius and (b) the parameter of j_0 at the onset of the buckling of nanowires with a fixed end and a pinned end

3. Critical length of nanowires with radial diffusion

Chakraborty et al. (Chakraborty et al., 2015) found that there is a critical length below which a cylinder will never buckle no matter how large the axial force is. Such behavior is due to the continuous increase of the cylinder radius induced by diffusion-induced expansion. They performed numerical calculation to evaluate the critical length of silicon nanowires for several influx rates without providing any analytical solution. It is always desirable to have closed-form solutions in analyzing the effects of parameters on the critical length, which can provide the design criteria for the use of nanowire-based electrodes.

It is known that it is very difficult, if not impossible, to obtain closed-form solutions from the theory of large deformation. Numerical analysis was used to compare the numerical results with the closed-form solutions derived from the theory of linear elasticity and to assess the applicability of the closed-form solutions in determining the critical load from the theory of large deformation. The governing equations for diffusion-induced buckling in the theory of linear elasticity are summarized in Appendix B. The following summaries the results.

Figure 6 shows the comparison between the results obtained from the theory of large deformation and those from the theory of linear elasticity. Here, nanowires were fixed at one

end and pinned at the other end. The solid lines represent the results from the theory of large deformation, and the squares represent the results from the theory of linear elasticity. The critical buckling time decreases nonlinearly with increasing the value of j_0, independent of the theory used. For nanowires with small ratios of length to radius, the critical buckling time calculated from the theory of large deformation is slightly larger than that calculated from the theory of linear elasticity for the same value of j_0. This trend reveals the effect of the cross-section on the critical load for the onset of the buckling. For nanowires with large ratios of length to radius ($L/R_0 \geq 10$), there is no observable difference between the critical buckling times calculated from the theory of large deformation and the theory of linear elasticity, respectively. For nanowires with small ratios of length to radius ($L/R_0 < 10$), there exists observable difference between these two results. Such behavior suggests that a nanowire with a small aspect ratio can withstand a larger axial, compressive force before the onset of the buckling, i.e. the nanowire can experience relatively large deformation and stresses. Under such a condition, the theory of large deformation is more applicable in describing the deformation behavior of the nanowire.

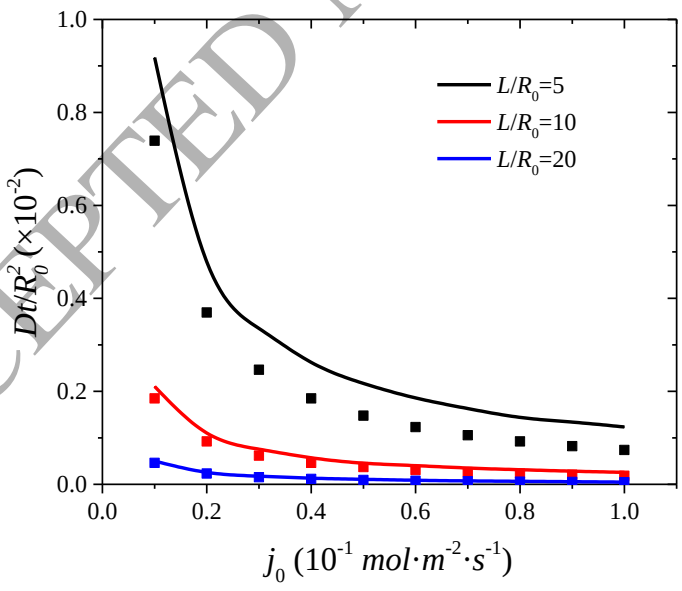

Figure 6. Comparison of the variation of the critical buckling times with j_0 for the onset of the buckling of nanowires with different ratios of length to radius (Solid lines represent the results from the theory of large deformation; squares represent the results from the theory of linear elasticity. Nanowires were fixed at one end and pinned at the other end.)

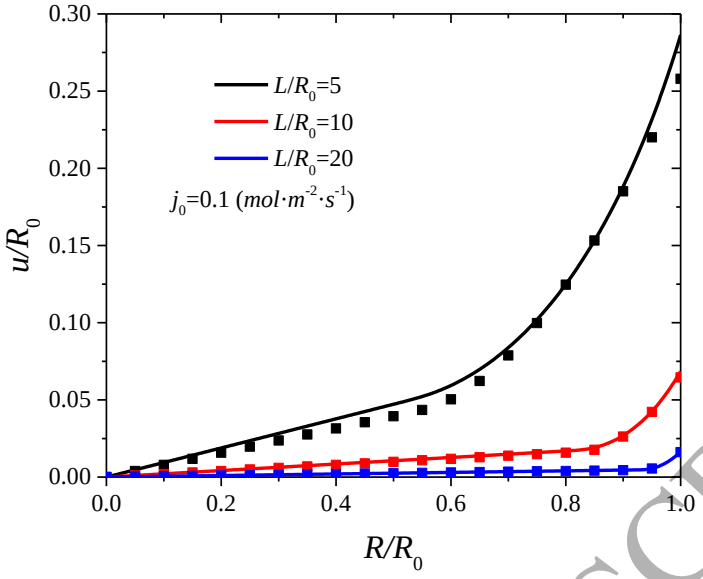

Figure 7. Spatial variation of the radial displacement at the onset of the buckling of nanowires with different ratios of length to radius (Solid lines represent the results from the theory of large deformation; squares represent the results from the theory of linear elasticity. Nanowires were fixed at one end and pinned at the other end.)

To further explore the difference between the deformations calculated from these two theories, the spatial variation of the radial displacement calculated from both theories at the onset of buckling is depicted in Fig. 7 for three different ratios of length to radius. Here, nanowires were fixed at one end and pinned at the other end. The radial displacement is zero at the axisymmetric axis of the nanowire (R/R_0=0) and increases with R (R/R_0), and reaches the maximum at the surface of the nanowire (R/R_0=1) for all three nanowires. For nanowires with small ratios of length to radius and the same value of j_0, the radial displacement calculated from the theory of large deformation is slightly larger than that calculated from the theory of linear elasticity. For nanowires with large ratios of length to radius ($L/R_0 \geq 10$), there is no observable difference between the radial displacement calculated from the theory of large deformation and that from the theory of linear elasticity, respectively. The radial displacement at the surface of the nanowire (R/R_0=1) decreases with the increase of the length of nanowires of the same radius at the onset of buckling. This result is in accord with the observation that a shorter nanowire can accommodate a larger amount of solute atoms and experience a larger compressive force before the occurrence of buckling according to Eq.

(23), which results in a larger expansion of the nanowire in the radial direction. The differences in the radial displacements (u/R_0) at the surface of the nanowires with L/R_0 = 5, 10 and 20 are 9.91%, 5.87% and 2.39%, respectively.

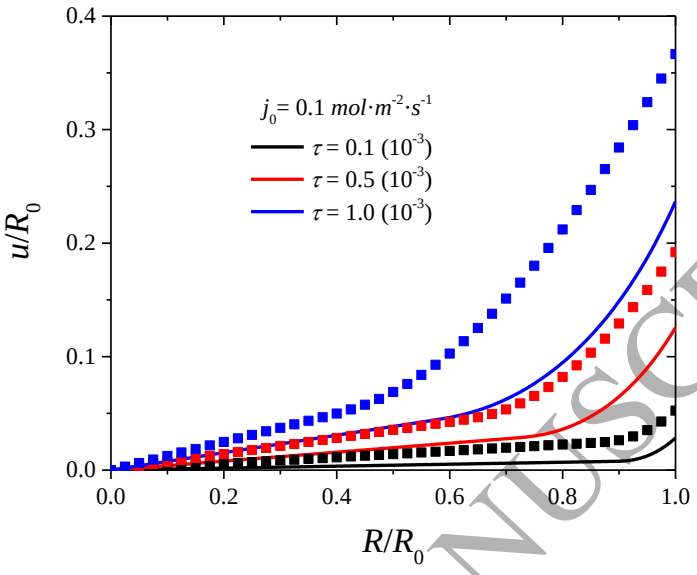

Figure 8. Spatial variation of the radial displacement of a nanowire at different lithiation times (Solid lines represent the results from the theory of large deformation; squares represent the results from the theory of linear elasticity. Nanowire was fixed at one end and pinned at the other end.)

To understand the difference between the critical buckling times calculated from the two theories, the spatial variation of the radial displacement at different lithiation times is shown in Fig. 8. There exists significant difference between the radial displacements calculated from the two theories at the same lithiation time. For the dimensionless lithiation time $\tau = 1.0\times10^{-3}$, the difference between the radial displacements is 35.40%. Such behavior can be readily analyzed from the elastic theory of large deformation.

Consider the radial strain of Eq. (9) in the elastic theory of large deformation. The Taylor series expansion of the radial strain, E_R^e, gives

$$E_R^e \approx \frac{\partial u}{\partial R} - \frac{1}{3}\Omega C - \frac{2}{3}\frac{\partial u}{\partial R}\Omega C . \qquad (43)$$

From the theory of linear elasticity, the radial strain, ε_R^e, is calculated as

$$\varepsilon_R^e = \frac{\partial u}{\partial R} - \frac{1}{3}\Omega_1 C. \tag{44}$$

Substituting Eq. (44) into Eq. (43), one obtains

$$E_R^e \approx \varepsilon_R^e - \frac{2}{3}\frac{\partial u}{\partial R}\Omega_1 C \tag{45}$$

To the first order approximation, the difference of the radial strains between the large deformation and small deformation is proportion to the volumetric strain associated with the diffusion of solute atoms and the radial gradient of the radial displacement.

For the lithiation process, there is $\partial u/\partial R>0$, resulting in $E_R^e < \varepsilon_R^e$. The stress, strain and displacement results calculated from the theory of linear elasticity are larger than those from the elastic theory of large deformation at the same lithiation time, leading to that the nanowire quickly reaches the critical state for the onset of buckling. This result reveals that the theory of linear elasticity underestimates the critical buckling time induced by the diffusion of solute atoms due to the negligence of the higher order terms in the diffusion-induced strain and the nonlinear terms in strain tensor.

All of the results suggest that both theories give the same trend; the theory of large deformation likely gives more complete results, and the use of the theory of linear elasticity can approximately provide the critical buckling time. Thus, the analysis based on the theory of linear elasticity is used to determine the critical length of nanowires, below which there is no occurrence of buckling.

From the governing equations for the diffusion-induced buckling in the theory of linear elasticity in Appendix B, one can determine the critical amount of solute atoms in a nanowire for the onset of buckling as

$$\frac{2}{3}E_h\Omega_1\pi\int_0^{R_0} CRdR = \frac{\pi^2 E_h I}{(\chi L)^2}. \tag{46}$$

Denote t_b as the critical buckling time. The corresponding critical *SOC* at the onset of buckling, $SOC_{buckling}$, can be expressed as

$$SOC_{buckling} = \frac{2\int_0^{R_0} C(R,t_b)RdR}{C_{\max}R_0^2}. \tag{47}$$

Substituting Eq. (47) into Eq. (46) yields the *SOC* at the onset of buckling of a nanowire as

$$SOC_{buckling} = \frac{3\pi^2}{4\chi^2 \left(L/R_0\right)^2 \Omega_1 C_{\max}}, \tag{48}$$

where L/R_0 is the dimensionless length of the nanowire, and $\Omega_1 C_{\max}$ is the volumetric strain at the fully lithiated state.

Equation (48) represents the relationship among *SOC* at the onset of buckling, effective length factor of χ, dimensionless length, and the volumetric strain at the fully lithiated state. One can calculate one of the parameters if other three parameters are given. For example, one obtains the critical *SOC* of 2.47% for the onset of buckling for a silicon nanowire of a length of $20R_0$ with the fixed condition at both ends since the effective length factor of χ is 0.5 and $\Omega_1 C_{\max}$ at the fully lithiated state is 3 (Zhao et al., 2011).

It is known that *SOC* can vary from 0% to 100%. Thus, the state with *SOC*=100% represents the critical state for the possible occurrence of buckling, and the critical length of a nanowire, L_{cr}, below which no buckling can occur, is found as

$$L_{cr}/R_0 = \frac{\pi}{2\chi}\sqrt{\frac{3}{\Omega_1 C_{\max}}}, \tag{49}$$

The critical length is proportional to the initial radius of the nanowire and inversely proportional to the square root of the volumetric strain at the fully lithiated state. Note that the critical length is independent of the influx value due to the use of the fully lithiated state, and is the upper bound within the framework of linear elasticity.

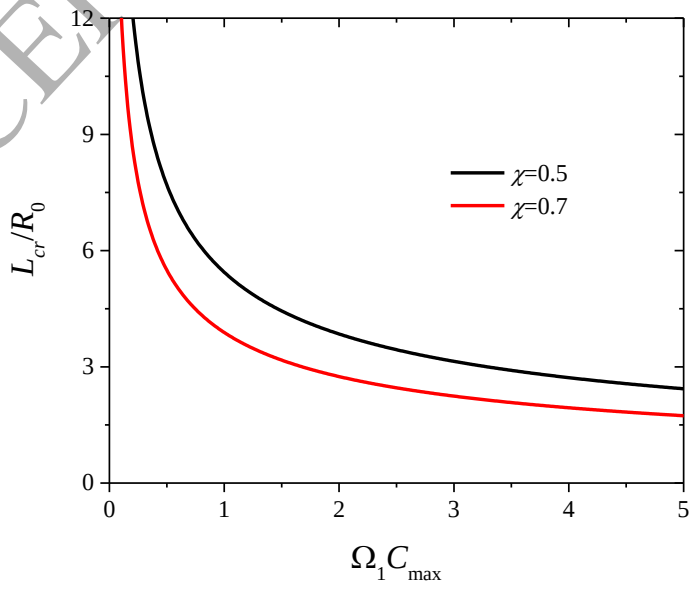

Figure 9. Variation of the critical length with the volumetric strain at fully lithiated state for two different constraints to the ends of a nanowire

Figure 9 shows the variation of the critical lengths with the volumetric strain at the fully lithiated state for two different constraints to the ends of a nanowire. It is evident that the critical length decreases with the increase of the volumetric strain at the fully lithiated state, suggesting that the radial expansion can mitigate the occurrence of the buckling of the nanowire. A nanowire with two fixed ends has a larger critical length than the same nanowire with a fixed end and a pinned end for the same value of $\Omega_1 C_{\max}$. For a silicon nanowire with two fixed ends and $\Omega_1 C_{\max} = 3$, the critical length is $3.14R_0$.

Chakraborty et al. (Chakraborty et al., 2015) proposed a modified Euler's critical load to determine the critical length below which no buckling will ever occur. Their proposed formula can be expressed as

$$F_{cr}^{m} = -\frac{\pi^2 E_h I_{CF}}{(\chi L)^2}, \text{ and } I_{CF} = \pi\left(R_0\left(1+\frac{\partial u}{\partial R}\right)\right)^4/4 \tag{50}$$

where I_{CF} is the inertia moment of the nanowire in the current configuration. This modified buckling criterion may be more suitable for determining the critical length of nanowires with large deformation. In the theory of linear elasticity, the inertia moment of a deformed nanowire is

$$I_{CF} = \frac{1}{4}\pi\left(R_0 + u\big|_{R=R_0}\right)^4. \tag{51}$$

Substituting the expression of the radial displacement, u, in Appendix B into Eq. (51), one obtains

$$I_{CF} = \frac{1}{4}\pi R_0^4\left(1+\frac{2}{3}\Omega_1\frac{1+\nu}{R_0}\int_0^{R_0} CR dR\right)^4. \tag{52}$$

Substituting Eq. (42) into Eq. (52) yields

$$I_{CF} = \frac{1}{4}\pi R_0^4\left(1+\frac{1+\nu}{3}\Omega_1 C_{\max} SOC\right)^4. \tag{53}$$

Using Eq. (53) in Eq. (B-14), one obtains the nanowire length at the onset of the diffusion-induced buckling of a nanowire in terms of *SOC* as

$$\frac{L}{R_0}=\frac{\pi}{2\chi}\sqrt{\frac{\left(1+\frac{1}{3}\theta(1+\nu)\right)^4}{\frac{1}{3}\theta}}, \tag{54}$$

where $\theta=\Omega_1 C_{\max} SOC$, which represents the volumetric strain for a given *SOC*. The minimum value of L/R_0 of Eq. (54) can be found at $\theta=1/(1+\nu)$ from $\mathrm{d}(L/R_0)/\mathrm{d}\theta=0$. The critical length is

$$\frac{L_{cr}}{R_0}=\frac{8\pi}{3\sqrt{3}\chi}\sqrt{1+\nu}, \quad for \quad \Omega_1 C_{\max} SOC=\frac{1}{1+\nu}, \tag{55}$$

Note that *SOC* varies from 0 to 100%. Eq. (55) is valid only for $\Omega_1 C_{\max}\geq 1/(1+\nu)$. For $\Omega_1 C_{\max}<1/(1+\nu)$, the L/R_0 of Eq. (54) reaches minimum value at *SOC* = 1. Thus, the critical length can be summarized as

$$\frac{L_{cr}}{R_0}=\begin{cases}\dfrac{\pi}{2\chi}\sqrt{\dfrac{\left(1+\frac{1}{3}\Omega_1 C_{\max}(1+\nu)\right)^4}{\frac{1}{3}\Omega_1 C_{\max}}}, & for \quad \Omega_1 C_{\max}<\dfrac{1}{1+\nu} \\ \dfrac{8\pi}{3\sqrt{3}\chi}\sqrt{1+\nu}, & for \quad \Omega_1 C_{\max}\geq\dfrac{1}{1+\nu}\end{cases}. \tag{56}$$

According to Eq. (56), for $\Omega_1 C_{\max}<1/(1+\nu)$, a nanowire, which is shorter than the critical length, will be fully lithiated before the onset of buckling; for $\Omega_1 C_{\max}\geq 1/(1+\nu)$, a nanowire, which is shorter than the critical length, will never buckle when the increasing rate of the critical buckling load due to the increase of radius is greater than the increasing rate of the axial force induced by diffusion.

The variation of the critical lengths determined by the modified buckling criterion and the classical Euler's criterion with different volumetric strains at the fully lithiated state is shown in Fig. 10, taking ν as 0.28 and χ as 0.5. It is evident that the difference between the two critical lengths is negligible for small $\Omega_1 C_{\max}$, since the difference of the inertia moment between a deformed nanowire and an un-deformed nanowire is small. The difference between the two critical lengths increases with the increase of $\Omega_1 C_{\max}$ due to the increase of the inertia moment of the nanowire in the current configuration with the increase of $\Omega_1 C_{\max}$. Note that the numerical result of the critical length for silicon nanowires given by Chakraborty et al. (Chakraborty et al., 2015) is $35.6R_0$, which is significantly different from the results of $3.14R_0$ and $10.94R_0$ given by Eq. (49) and Eq. (56), respectively. Such differences are due to the use

of elastoplastic deformation in the buckling analysis by Chakraborty et al. (Chakraborty et al., 2015). The axial compressive force, which causes the buckling of a nanowire of a long length at the state of elastoplatic deformation, is smaller than that at the state of elastic deformation under the condition of the same *SOC*, resulting in the great difference in the critical lengths.

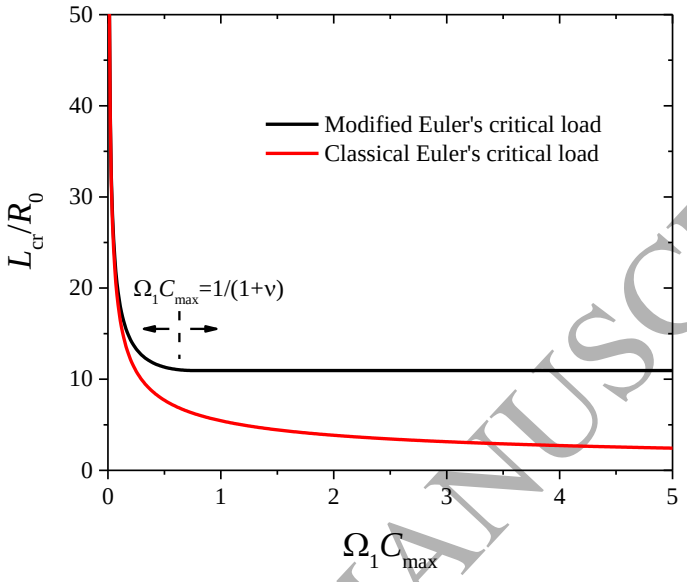

Figure 10. Variation of the critical lengths determined by the modified buckling criterion and classical Euler's criterion with volumetric strain at the fully lithiated state for nanowires with two fixed ends

Note that both the critical length and the critical buckling *SOC* of a nanowire are dependent on the critical load. For a nanowire with two fixed ends and L/R_0=11.5 subjected to an influx of j_0=0.1 $mol \cdot m^{-2} \cdot s^{-1}$, the critical buckling *SOC* is found to be 6.46% from the classical Euler's buckling load and 42.63% from the modified Euler's buckling load. Such a difference is due to the use of the nanowire radius at the deformed state in the calculation of the modified Euler's critical load, which allows the nanowire to withstand a large compressive, axial force before the onset of buckling. Thus, the nanowire can accommodate more lithium before the onset of buckling; the critical buckling *SOC* calculated from the modified Euler's critical load is then larger than that from the classical Euler's critical load.

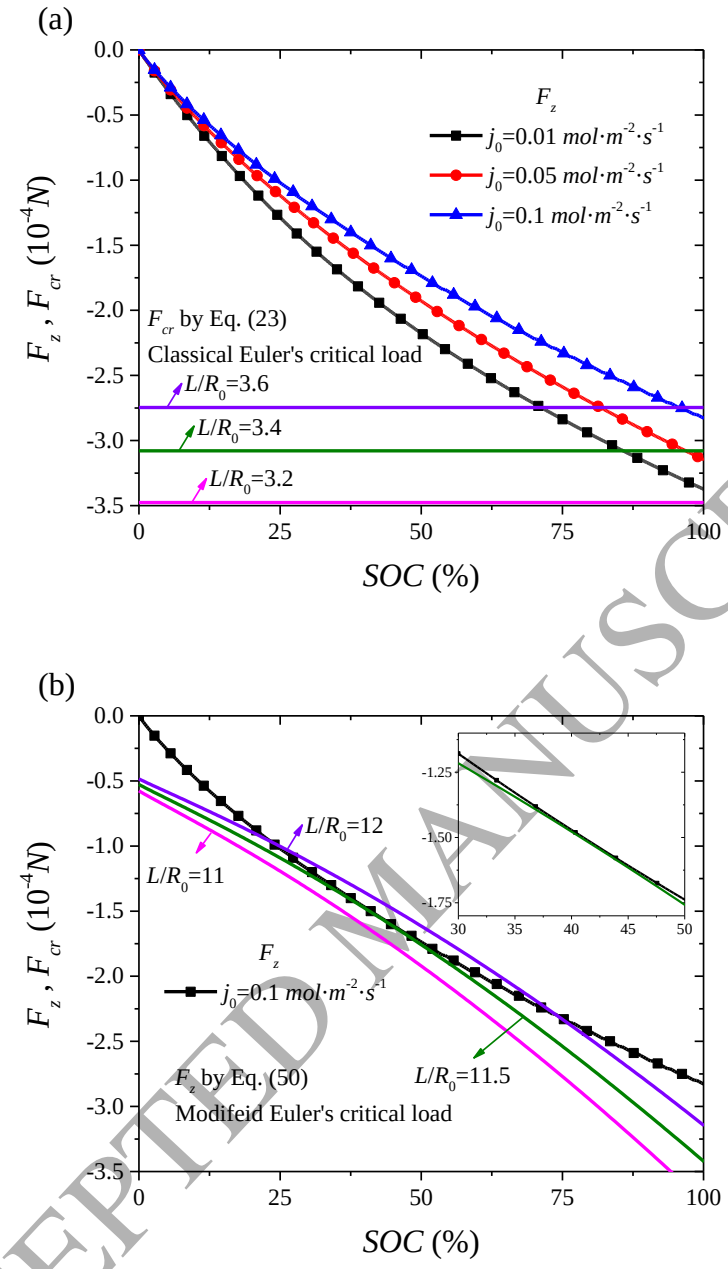

Figure 11. Variation of axial forces with *SOC* of nanowires with different influxes in comparison with (a) classical Euler's critical load, and (b) modified Euler's critical load. (Nanowires are fixed at two ends.)

As given in Eq. (56), the critical length, which is based on the theory of linear elasticity, is independent of the influx of j_0, while the influx may plays a role in determining the critical length if the theory of large deformation is considered. To evaluate the effect of the influx on the critical length, the variation of the axial force with *SOC* for nanowires subjected to different influxes and the variation of the critical buckling load with *SOC* for nanowires with

different aspect ratios are depicted Fig. 11. The critical length from the classical Euler's critical load can be determined, as shown in Fig. 11a, from the intersection between a critical load line and an axial force line at *SOC*=100%. From Fig. 11a, the critical lengths for nanowires with j_0=0.01 and j_0=0.1 are ~3.5R_0 and ~3.2R_0, respectively, which were calculated from the theory of large deformation by solving the governing equations in Sections 2.1 and 2.2 using COMSOL. The difference of the critical lengths is less than 10%, suggesting that the influence of surface flux on the critical length is relatively small. Also, the intersection of the curves of axial force with the line of the critical buckling load gives the *SOCs*, at which the buckling of nanowires occurs at the same buckling load. For example, the curve with black square intersects with the green line at *SOC* ≈ 87%, as shown in Fig 11a, suggesting that the nanowire with an aspect ratio of 3.4 will buckle at an axial load of 3.1×10^{-4} *N*, and the critical buckling *SOC* is about 87%.

The critical length from the modified Euler's critical load can be determined, as shown in the embedded figure in Fig. 11b, when a critical load curve is tangent to an axial force curve. From Fig. 11, the critical lengths for nanowires with j_0=0.1 $mol\cdot m^{-2}\cdot s^{-1}$ are ~3.5R_0 and ~11.5R_0, which were determined by the classical Euler's criterion and the modified buckling criterion, respectively. These values are compatible with 3.14R_0 and 10.94R_0 calculated from Eq. (49) and Eq. (56), respectively, which are based on the theory of linear elasticity without or with the consideration of the contribution of the change of the cross-sectional area of the nanowires. Using the method discussed above, the critical length as a function of the influx is calculated from the modified Euler's critical load and shown in Fig. 12. The critical length increases slightly with the increase of the value of the influx for j_0 less than 1 $mol\cdot m^{-2}\cdot s^{-1}$ and rapidly with the increase of the value of the influx for j_0 larger than 1 $mol\cdot m^{-2}\cdot s^{-1}$. This trend suggests that the theory of linear elasticity can be used to calculate the critical length calculated for the influx of j_0 less than 1 $mol\cdot m^{-2}\cdot s^{-1}$, if plastic deformation is negligible.

It needs to point out that the volumetric strain will lead to movement of the boundary of solid during the migration/diffusion of solute atoms, while boundaries are referred to the un-deformed state in the theory of linear elasticity. The relationship presented in Eq. (56) incorporates the movement of the boundary in the calculation of the critical length.

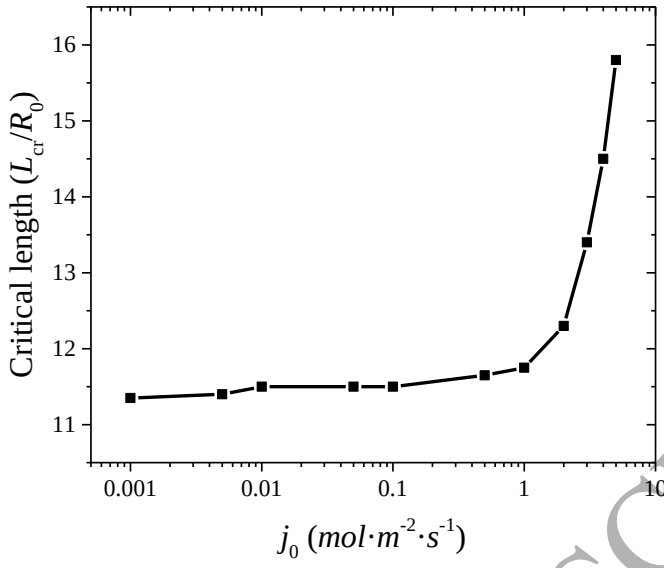

Figure 12. Effect of influx on the critical length calculated from the modified Euler's critical load (Nanowires are fixed at two ends.)

4. Diffusion-induced buckling of a nanowire with axial diffusion

The above analyses have been based on the diffusion path being in the radial direction. In general, there exists axial diffusion, as shown by Huang et al. (Huang et al., 2010) in the in-situ observation of the electrochemical lithiation of a single SnO_2 nanowire electrode. For the deformation due to axial diffusion of lithium, the approximation of plane strain is inapplicable. It is a three-dimensional problem, which is difficult to be solved analytically. Here, the diffusion-induced buckling of a nanowire with axial diffusion was analyzed numerically.

Figure 13 shows a nanowire of initial length of L and radius of R_0 with axial diffusion, i.e., lithium flows into the nanowire from top surface. Finite element software of ABAQUS with large deformation was used to analyze the diffusion-induced buckling of the nanowire with axial diffusion. A 3D finite element model of the nanowire was constructed, using 8-node fully integrated thermally coupled brick elements with the element size of $R_0/12$ in radial direction and $R_0/5$ in axial direction. The convergence of the FEM model has been checked to ensure the accuracy of the numerical calculation. The material properties and parameters used in the numerical analysis are listed in Table I.

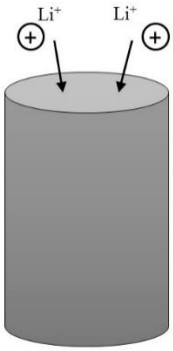

Figure 13. Schematic of a nanowire electrode with axial diffusion

Two steps were used in the numerical analysis to calculate the critical buckling time and analyze the post-buckling behavior. The first step calculates the buckling mode of the nanowire; the second step calculates the post-buckling deformation of the nanowire, using the buckling mode determined in the first step as an imperfection. In the second step, the onset of the buckling is determined when the resultant axial force is equal to the Euler's critical load given in Eq. (23), which is also validated in Appendix A.

For simplicity, the chemical potential used in the numerical analysis is assumed to be concentration-dependent only due to the difficulty in including the effect of stress on chemical potential of Eq. (29) in ABAQUS. The chemical potential reduces to

$$\mu = \mu_0 + R_g T \ln c, \tag{57}$$

and the diffusion problem is analogous to a problem of heat transfer. A transient coupled thermal-mechanical step in the FEM model was set for the post-buckling calculation.

In the simulation, lithium migrates into the nanowire from the fixed end (the bottom surface), and there are no fluxes from the other surfaces into the nanowire. For galvanostatic charging, the boundary condition for the bottom surface (fixed end) in the Eulerian description is

$$\mathbf{j}(\mathbf{x},t)\mathbf{n}\big|_{z=0} = \mathbf{j}_0\mathbf{n}, \quad t>0, \tag{58}$$

and the corresponding boundary condition in the Lagrangian description is

$$\mathbf{J}(\mathbf{X},t)\mathbf{N}\big|_{Z=0} = \det(\mathbf{F})\,\mathbf{j}_0\mathbf{F}^{-T}\mathbf{N}, \quad t>0, \tag{59}$$

The boundary condition for other surfaces in the Eulerian description is

$$\mathbf{j}(\mathbf{x}_0,t)\mathbf{n} = 0, \quad t>0, \tag{60}$$

and the corresponding boundary condition in the Lagrangian description is

$$\mathbf{J}(\mathbf{X}_0,t)\mathbf{N}=0,\quad t>0, \tag{61}$$

The initial condition for the nanowire without solute atoms incipiently in the Eulerian description is

$$c(\mathbf{x},0)=0,\quad 0<\mathbf{x}<\mathbf{x}_0(t), \tag{62}$$

and the corresponding initial condition in the Lagrangian description is

$$C(\mathbf{X},0)=0,\quad 0<\mathbf{X}<\mathbf{X}_0. \tag{63}$$

The nanowire is stress-free at t=0. There is no surface loading applied to the nanowire. One end of the nanowire is fixed, and the other is pinned.

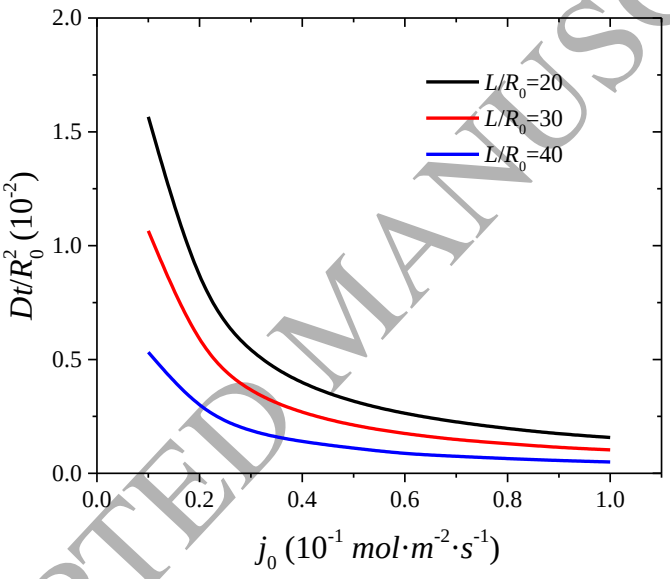

Figure 14. Variation of the critical buckling time with the influx of j_0 for the onset of the buckling of nanowires with different ratios of length to radius due to axial diffusion

Figure 14 shows the variation of the critical buckling time with the value of j_0 for nanowires of different lengths due to axial diffusion. It is evident that the critical buckling time decreases with the increasing value of j_0, as expected. The comparison of the critical buckling times between the axial-diffusion-controlled buckling and the radial-diffusion-controlled buckling shows that it requires a larger critical buckling time for a nanowire with axial diffusion than that for the same nanowire with radial diffusion. For example, the critical buckling time is 1.57×10^{-2} for a nanowire of L=20R_0 with the axial diffusion and 5.51×10^{-4} for the same nanowire with the radial diffusion for j_0=0.1 (10^{-1}

$mol \cdot m^{-2} \cdot s^{-1}$). The trend is due to the differences in the diffusion distance and the total area for the diffusion of lithium. More lithium can diffuse into the nanowire with the radial diffusion for the same diffusion time since the area of the side surface is much larger than the cross-sectional area.

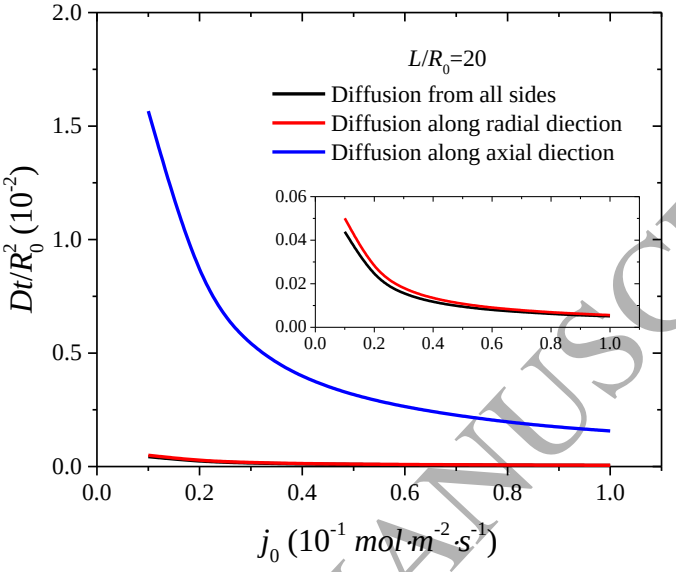

Figure 15. Variation of the critical buckling time with the parameter of j_0 for the onset of the buckling of a nanowire of L=20R_0 with different diffusion paths

In reality, diffusion can occur on all the surface of a suspended nanowire. Figure 15 shows the critical buckling time for a suspended nanowire of L/R_0=20 with the lithium migration into the nanowire on all surfaces. For comparison, the results with the axial diffusion or radial diffusion only are also included in Fig. 15. It is evident that the critical buckling time is the largest for the case with only axial diffusion (blue curve) due to the smallest surface area for the lithium diffusion, which requires the longest time for the axial, compressive force to reach the critical buckling load. There is no significant difference between the critical buckling time for the buckling controlled by the radial diffusion and that by the diffusion into all surfaces. The contribution from the axial diffusion is negligible in comparison with the radial diffusion for large ratio of length to radius.

Figure 16 shows the variation of the critical buckling time with the ratio of length to radius for a nanowire with different diffusion paths. Note that the critical length is ~10R_0, so the aspect ratios in the result were selected from 10L/R_0 to 15L/R_0. The contribution from the

diffusion in axial direction is negligible even for small aspect ratio, and the critical buckling time change slightly with the increasing aspect ratio, owning to the small end surface in comparison with the side surface.

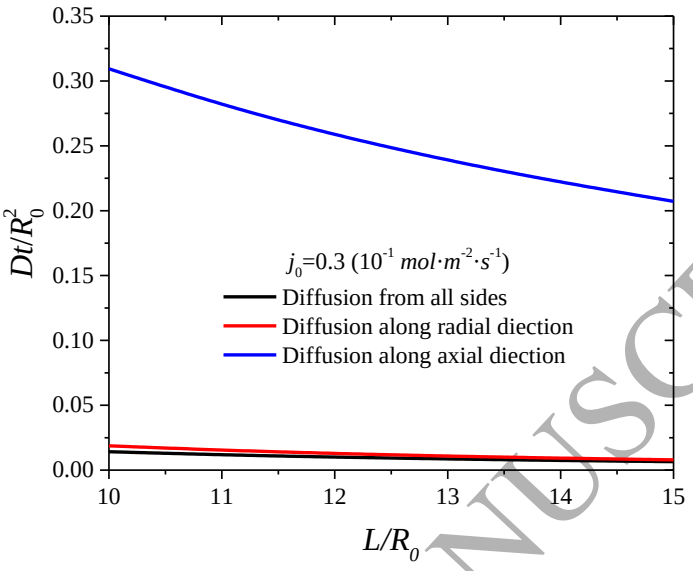

Figure 16. Variation of the critical buckling time with the ratio of length to radius for the onset of the buckling of a nanowire with different diffusion paths

5. Summary

In summary, this study is focused on the diffusion-induced buckling of nanowires. The elastic theory of large deformation has been incorporated in analyzing the diffusion-induced buckling of the nanowires with radial diffusion. Numerical analyses have been performed to examine the dependence of the critical buckling time on the nanowire length, current density, and constraint to the motion of the ends of the nanowires. The numerical results show that the critical buckling time decreases with the increase of the nanowire length or current density with different mechanisms. The increase of the nanowire length reduces the Euler's critical load for the onset of buckling, while the increase of the current density causes the increase of the axial, compressive force. A nanowire with two fixed end has a larger critical buckling time than that for the nanowire of the same length with a fixed end and a pinned end. Both the aspect ratio of a nanowire and current density play important roles in determining the critical *SOC* for the onset of buckling. Analytical solution for the critical length of a nanowire with radial diffusion, below which there is no buckling, has been obtained, using the model

from the theory of linear elasticity. The critical length is dependent on the constraints to the ends of the nanowire and the volumetric strain at the fully lithiated state. This analytical solution is compared with the numerical results from the elastic theory of large deformation, and the result shows that the analytical solution is valid for the influx less than 1 $mol \cdot m^{-2} \cdot s^{-1}$ and configurations considered in the work.

Finite element method has been used to analyze the diffusion-induced buckling of nanowires with axial diffusion. The critical buckling time decreases with the increasing value of j_0 and the ratio of length to radius, similar to the results with radial diffusion. It needs a larger critical buckling time for a nanowire with axial diffusion than that for the same nanowire with radial diffusion. For nanowires of large ratios of length to radius with diffusion from all surfaces, the contribution from the axial diffusion is negligible in comparison with the radial diffusion even for small aspect ratio, and the critical buckling time does not change a lot with the increasing aspect ratio

Appendix A: Post-buckling Analysis of a Nanowire

A 3D finite element model of a nanowire with a radius of R_0 and a length of $30R_0$ was constructed. The material properties of the nanowire are listed in Table I. One end of the nanowire is fixed (i.e. all 3 translational DOF and 3 rotational DOF are zero), and the other end is pinned (all 3 translational DOF are zero). The nanowire is subjected to a surface flux either on the side surface or on the bottom surface. The value of j_0 is 0.1 (10^{-4} $mol{\cdot}m^{-2}{\cdot}s^{-1}$). For the axial diffusion, lithium migrates from the fixed end into the nanowire, and there are no fluxes on other surfaces. A linear buckle analysis was firstly performed to obtain the buckling mode of the first order, which was used as the imperfection in analyzing the post-buckling of the nanowire. Here, the stress terms in the chemical potential of Eq. (29) are neglected in the finite element analysis due to the difficulty in incorporating the stress terms in the finite element code. The chemical potential used in the analysis is expressed as

$$\mu = \mu_0 + R_g T \ln c, \tag{A-1}$$

As discussed above, the diffusion problem is analogous to a problem of heat transfer. Thus, a transient coupled thermal-mechanical analysis with 8-node fully integrated thermally coupled brick elements was performed.

Figure A1 shows the temporal evolution of the resultant axial force in the nanowire. The solid line represents the result obtained from the FEA simulation, and the black squares represent the numerical result (Fig. A1a) obtained from the solutions of the equations in Section 2.1 and 2.2 using the PDE module in COMSOL. The dashed line represents the linear extension of the COMSOL result (Fig. A1a) using the same chemical potential in Eq. (A-1) and the linear extension of the linear portion of the ABAQUS result (Fig. A1b). The red square in Fig. A1a represents the Euler's critical load calculated from Eq. (25) using the concentration-dependent chemical potential of Eq. (A-1). The red square in Fig. A1b represents the Euler's critical load, which was calculated from Eq. (B-14). It is evident that the Euler's critical load represents the critical load at which the resultant axial force becomes a nonlinear function of time (Figs. A1a and A1b), i.e. the initiation of the buckling. These results validate that the Euler's critical load can be used to determine the critical diffusion time for the onset of the diffusion-induced buckling of a nanowire.

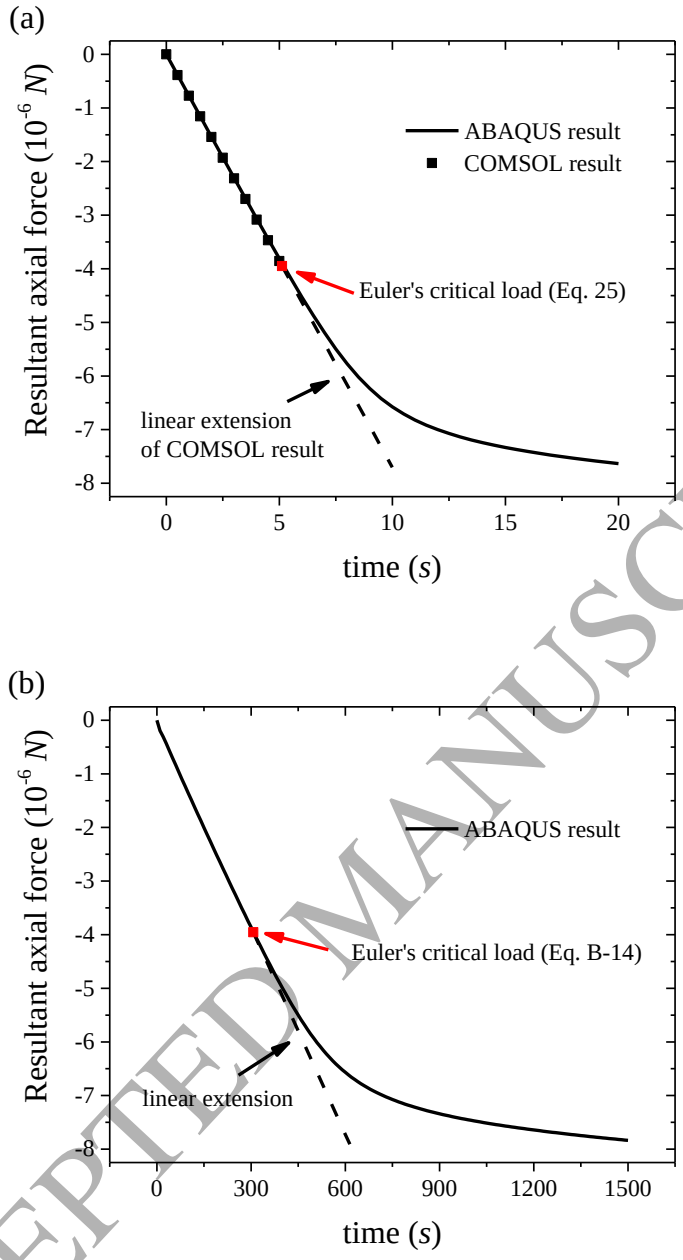

Figure A1. Temporal evolution of resultant axial force in a nanowire with (a) radial diffusion and (b) axial diffusion

Appendix B: Governing equations for diffusion-induced buckling of a nanowire in the theory of linear elasticity

Consider a nanowire in a cylindrical coordinate system (R, Θ, Z). The constitutive equation in the theory of linear elasticity can be written as

$$\varepsilon_R = \frac{1}{E_h}\left[\sigma_R - \nu\left(\sigma_\Theta + \sigma_Z\right)\right] + \frac{\Omega_1 C}{3}, \tag{B-1}$$

$$\varepsilon_\Theta = \frac{1}{E_h}\left[\sigma_\Theta - \nu\left(\sigma_R + \sigma_Z\right)\right] + \frac{\Omega_1 C}{3}, \tag{B-2}$$

$$\varepsilon_Z = \frac{1}{E_h}\left[\sigma_Z - \nu\left(\sigma_R + \sigma_\Theta\right)\right] + \frac{\Omega_1 C}{3}, \tag{B-3}$$

where ε_i and σ_i (i = R, Θ, Z) are the strain components and stress components, respectively. The strain components are calculated from the derivatives of the radial displacement, u, and the axial displacement, w, as

$$\varepsilon_R = \frac{\partial u}{\partial R}, \quad \varepsilon_\Theta = \frac{u}{R}, \quad \varepsilon_Z = \frac{\partial w}{\partial Z}. \tag{B-4}$$

The equilibrium equation in the absence of body force is

$$\frac{d\sigma_R}{dR} + \frac{\sigma_R - \sigma_\Theta}{R} = 0. \tag{B-5}$$

From the theory of linear elasticity (Timoshenko and Goodier, 1970), one obtains the radial displacement and axial displacement as

$$u = \frac{1+\nu}{1-\nu}\frac{\Omega_1}{3}\frac{1}{R}\int_0^R CR dR + AR + \frac{B}{R}, \quad \frac{\partial w}{\partial Z} = q, \tag{B-6}$$

where A, B and q are constants to be determined from the boundary conditions. The stress components, in terms of A, B and q, are

$$\sigma_R = -\frac{\Omega_1 E_h}{3(1-\nu)}\frac{1}{R^2}\int_0^R CR dR + \frac{E_h(A+\nu q)}{(1+\nu)(1-2\nu)} - \frac{E_h B}{(1+\nu)R^2}, \tag{B-7}$$

$$\sigma_\Theta = \frac{\Omega_1 E_h}{3(1-\nu)}\frac{1}{R^2}\int_0^R CR dR + \frac{E_h(A+\nu q)}{(1+\nu)(1-2\nu)} + \frac{E_h B}{(1+\nu)R^2} - \frac{E_h \Omega_1 C}{3(1-\nu)}, \tag{B-8}$$

$$\sigma_Z = \frac{2E_h \nu}{(1+\nu)(1-2\nu)}A - \frac{\Omega_1 E_h}{3(1-\nu)}C + \frac{E_h(1-\nu)}{(1+\nu)(1-2\nu)}q. \tag{B-9}$$

For a nanowire with length much larger than radius, the stress state of the nanowire can be approximated as plane strain, which gives q=0. The finite value of the radial displacement in

the nanowire gives B=0. The traction-free condition on the surface of the nanowire gives

$$\sigma_R\big|_{R=R_0} = 0, \tag{B-10}$$

from which one obtains

$$A = \Omega_1 \frac{(1+\nu)(1-2\nu)}{3(1-\nu)} \frac{1}{R_0^2} \int_0^{R_0} CRdR. \tag{B-11}$$

and the axial stress, σ_Z, as

$$\sigma_Z = \frac{2\Omega_1 E_h \nu}{3(1-\nu) R_0^2} \int_0^{R_0} CRdR - \frac{\Omega_1 E_h}{3(1-\nu)} C. \tag{B-12}$$

The resultant force, F_Z, acting on the nanowire in the axial direction is calculated from Eq. (B-12) as

$$F_Z = \int_0^{2\pi} \int_0^{R_0} \sigma_Z RdRd\Theta = -\frac{2}{3} E_h \Omega_1 \pi \int_0^{R_0} CRdR. \tag{B-13}$$

Substituting Eq. (B-13) into Eq. (24) yields

$$\frac{2}{3} E_h \Omega_1 \pi \int_0^{R_0} CRdR = \frac{\pi^2 E_h I}{(\chi L)^2}, \tag{B-14}$$

which determines the condition for the onset of the diffusion-induced buckling of a nanowire.

The mass transport equation in the cylindrical coordinate system (R, Θ, Z) is

$$\frac{\partial C(R,t)}{\partial t} + \frac{\partial \left(RJ(R,t)\right)}{R\partial R} = 0. \tag{B-15}$$

and the diffusion flux is

$$J = -MC \frac{\partial \mu}{\partial R}. \tag{B-16}$$

Substituting the stress components, the strain components, and Eq. (29) into Eq. (33), one obtains

$$J = -D\left(\frac{\partial C}{\partial R} - \frac{\Omega_1 C}{R_g T} \frac{\partial}{\partial R} \frac{\sigma_R + \sigma_\Theta + \sigma_Z}{3} + \frac{\Omega_2 C}{R_g T} \frac{\partial}{\partial R} \frac{\sigma_R \varepsilon_R + \sigma_\Theta \varepsilon_\Theta + \sigma_Z \varepsilon_Z}{2} \right). \tag{B-17}$$

The initial and boundary conditions corresponding to galvanostatic charging are

$$C(R,0) = 0, \quad 0 < R < R_0, \tag{B-18}$$

$$J(R_0,t) = j_0. \tag{B-19}$$

Substituting the solution of the diffusion equation into Eq. (B-14), one can calculate the

critical buckling time and critical concentration distribution of lithium.

Appendix C: Comparison of linear and non-linear Euler formulas

De Pascalis et al. (De Pascalis et al., 2011) gave the expression of the non-linear correction to the Euler formula for compressed cylinders with guided-guided end conditions, which is written as

$$\frac{N_{cr}}{\pi^3 R_0^2} = \frac{E_h}{4}\left(\frac{R_0}{L}\right)^2 - \frac{\pi^2}{96}\delta_{NL}\left(\frac{R_0}{L}\right)^4, \tag{C1}$$

where

$$\delta_{NL} = 2\frac{13+12\nu-2\nu^2}{1+\nu}E_h + 12\left(\left(1-2\nu^3\right)\mathcal{A} + 3\left(1-2\nu\right)\left(1+2\nu^2\right)\mathcal{B} + \left(1-2\nu\right)^3\mathcal{C}\right) \tag{C2}$$

with $\mathcal{A}$, $\mathcal{B}$ and $\mathcal{C}$ being the Landau constants.

Figure C1 shows the variations of the critical load with the ratio of length to radius for the buckling of a slender structure using the material parameters given in Table II collected by Porubov (Porubov, 2003). Here, Eq. (23) and Eq. (C1) were used respectively to calculate the critical load. The results show that difference between the results calculated respectively from these two formulas is negligible for the ratio of length to radius being larger than 5.

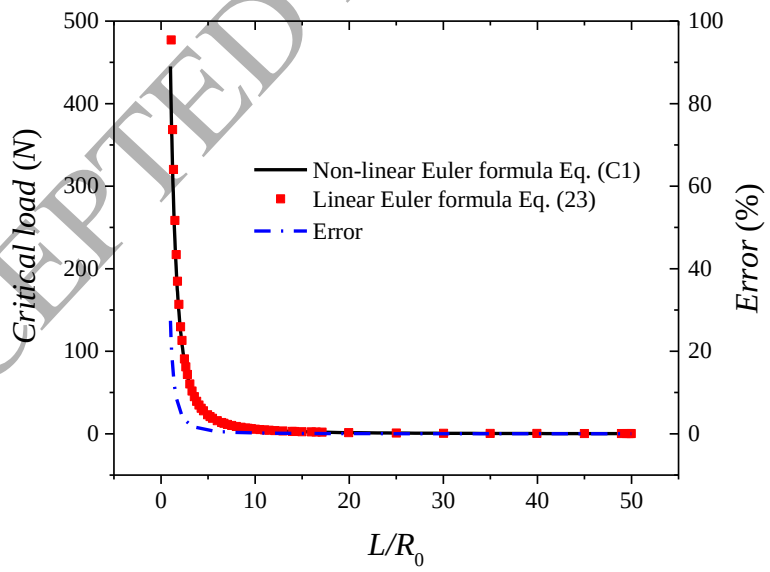

Figure C1. Variations of the critical load with the ratio of length to radius for the buckling of a slender structure

Table II. Young's Module, Poisson's ratio and Landau third-order elastic moduli for silica (10^9 $N \cdot m^{-2}$)

Material	E_h	v	$\mathcal{A}$	$\mathcal{B}$	$\mathcal{C}$
Silica	73.14	0.1684	-44	93	36

References:

Areias, P., Samaniego, E., Rabczuk, T., 2016. A staggered approach for the coupling of Cahn–Hilliard type diffusion and finite strain elasticity. Computational Mechanics 57, 339-351.

Barai, P., Mukherjee, P.P., 2016. Mechano-Electrochemical Stochastics in High-Capacity Electrodes for Energy Storage. Journal of The Electrochemical Society 163, A1120-A1137.

Bhandakkar, T.K., Gao, H., 2010. Cohesive modeling of crack nucleation under diffusion induced stresses in a thin strip: Implications on the critical size for flaw tolerant battery electrodes. International Journal of Solids and Structures 47, 1424-1434.

Bhandakkar, T.K., Johnson, H.T., 2012. Diffusion induced stresses in buckling battery electrodes. Journal of the Mechanics and Physics of Solids 60, 1103-1121.

Brassart, L., Zhao, K., Suo, Z., 2013. Cyclic plasticity and shakedown in high-capacity electrodes of lithium-ion batteries. International Journal of Solids and Structures 50, 1120-1129.

Chakraborty, J., Please, C.P., Goriely, A., Chapman, S.J., 2015. Combining mechanical and chemical effects in the deformation and failure of a cylindrical electrode particle in a Li-ion battery. International Journal of Solids and Structures 54, 66-81.

Chan, C.K., Peng, H., Liu, G., Mcllwrath, K., Zhang, X.F., Huggins, R.A., Cui, Y., 2008. High-performance lithium battery anodes using silicon nanowires. Nature nanotechnology 3, 31-35.

Cheng, Y.-T., Verbrugge, M.W., 2008. The influence of surface mechanics on diffusion induced stresses within spherical nanoparticles. J Appl Phys 104, 083521.

Cui, Y., 2011. Nanowire Lithium-Ion Batteries as Electrochemical Energy Storage for Electric Vehicles. Standford University.

Cui, Z., Gao, F., Qu, J., 2012. A finite deformation stress-dependent chemical potential and its applications to lithium ion batteries. Journal of the Mechanics and Physics of Solids 60, 1280-1295.

Cui, Z., Gao, F., Qu, J., 2013. Interface-reaction controlled diffusion in binary solids with applications to lithiation of silicon in lithium-ion batteries. Journal of the Mechanics and Physics of Solids 61, 293-310.

Damle, S.S., Pal, S., Kumta, P.N., Maiti, S., 2016. Effect of silicon configurations on the

mechanical integrity of silicon–carbon nanotube heterostructured anode for lithium ion battery: A computational study. Journal of Power Sources 304, 373-383.

De Pascalis, R., Destrade, M., Goriely, A., 2011. Nonlinear correction to the Euler buckling formula for compressed cylinders with guided-guided end conditions. Journal of Elasticity 102, 191-200.

Drozdov, A., 2014. Constitutive equations for self-limiting lithiation of electrode nanoparticles in Li-ion batteries. Mechanics Research Communications 57, 67-73.

Fyrillas, M.M., Nomura, K.K., 2007. Diffusion and Brownian motion in Lagrangian coordinates. The Journal of chemical physics 126, 164510.

Gao, F., Hong, W., 2016. Phase-field model for the two-phase lithiation of silicon. Journal of the Mechanics and Physics of Solids 94, 18-32.

Gere, J.M., Goodno, B.J., 2009. Mechanics of materials. Cengage Learning.

Grushka, E., Grinberg, N., 2014. Advances in chromatography. CRC Press.

Huang, J.Y., Zhong, L., Wang, C.M., Sullivan, J.P., Xu, W., Zhang, L.Q., Mao, S.X., Hudak, N.S., Liu, X.H., Subramanian, A., 2010. In situ observation of the electrochemical lithiation of a single SnO2 nanowire electrode. Science 330, 1515-1520.

Larché, F., 1996. What can the concept of a perfect chemoelastic solid tell us about the mechanical and thermodynamic behaviour of a solid? Le Journal de Physique IV 6, C1-03-C01-09.

Larché, F., Cahn, J.W., 1985. Overview no. 41 the interactions of composition and stress in crystalline solids. Acta Metallurgica 33, 331-357.

Li, J.C.-M., 1978. Physical chemistry of some microstructural phenomena. Metallurgical Transactions A 9, 1353-1380.

Li, Y., Zhang, K., Zheng, B., Yang, F., 2016. Effect of local velocity on diffusion-induced stress in large-deformation electrodes of lithium-ion batteries. Journal of Power Sources 319, 168-177.

Liu, X.H., Fan, F., Yang, H., Zhang, S., Huang, J.Y., Zhu, T., 2013. Self-limiting lithiation in silicon nanowires. Acs Nano 7, 1495-1503.

Liu, Y., Hudak, N.S., Huber, D.L., Limmer, S.J., Sullivan, J.P., Huang, J.Y., 2011. In situ transmission electron microscopy observation of pulverization of aluminum nanowires and

evolution of the thin surface Al2O3 layers during lithiation–delithiation cycles. Nano letters 11, 4188-4194.

Pal, S., Damle, S.S., Patel, S.H., Datta, M.K., Kumta, P.N., Maiti, S., 2014. Modeling the delamination of amorphous-silicon thin film anode for lithium-ion battery. Journal of Power Sources 246, 149-159.

Porubov, A.V., 2003. Amplification of nonlinear strain waves in solids. World Scientific.

Prussin, S., 1961. Generation and distribution of dislocations by solute diffusion. Journal of Applied Physics 32, 1876-1881.

Timoshenko, S., Goodier, J., 1970. Theory of Elasticity (3rd) McGraw-Hill. New York.

Wang, M., Xiao, X., 2016. Investigation of the chemo-mechanical coupling in lithiation/delithiation of amorphous Si through simulations of Si thin films and Si nanospheres. Journal of Power Sources 326, 365-376.

Yang, F.Q., 2010. Effect of local solid reaction on diffusion-induced stress. Journal of Applied Physics 107, 103516.

Yang, F.Q., 2005. Interaction between diffusion and chemical stresses. Mat Sci Eng a-Struct 409, 153-159.

Zhang, J.L., Zhao, Y.P., 2012. A diffusion and curvature dependent surface elastic model with application to stress analysis of anode in lithium ion battery. Int J Eng Sci 61, 156-170.

Zhang, X., Sastry, A.M., Shyy, W., 2008. Intercalation-induced stress and heat generation within single lithium-ion battery cathode particles. Journal of The Electrochemical Society 155, A542-A552.

Zhang, X., Shyy, W., Sastry, A.M., 2007. Numerical simulation of intercalation-induced stress in Li-ion battery electrode particles. Journal of the Electrochemical Society 154, A910-A916.

Zhao, K., Pharr, M., Cai, S., Vlassak, J.J., Suo, Z., 2011. Large Plastic Deformation in High-Capacity Lithium-Ion Batteries Caused by Charge and Discharge. Journal of the American Ceramic Society 94, s226-s235.

Zhong, L., Liu, X.H., Wang, G.F., Mao, S.X., Huang, J.Y., 2011. Multiple-stripe lithiation mechanism of individual SnO 2 nanowires in a flooding geometry. Physical review letters 106, 248302.